NSRRC - J05315 (2016)

CHEMISTRY OF MATERIALS

Article

pubs.acs.org/cm

Understanding Morphology Compatibility for High-Performance Ternary Organic Solar Cells

Jiangquan Mai,[†] Tsz-Ki Lau,[†] Jun Li,[‡] Shih-Hao Peng,[§] Chain-Shu Hsu,[§] U-Ser Jeng,[#] Jianrong Zeng,[∥] Ni Zhao,[⊥] Xudong Xiao,[†] and Xinhui Lu*[,†]

[†]Department of Physics, The Chinese University of Hong Kong, New Territories, Hong Kong

[‡]Department of Chemistry and Centre for Plastic Electronics, Imperial College London, London SW 7 2AZ, United Kingdom

[§]Department of Applied Chemistry, National Chiao Tung University, Hsinchu, Taiwan

[#]National Synchrotron Radiation Research Center, 101 Hsin-Ann Road, Hsinchu Science Park, Hsinchu, Taiwan

[∥]Shanghai Synchrotron Radiation Facility, 239 Zhangheng Road, Pudong New District, Shanghai, China

[⊥]Department of Electronic Engineering, Chinese University of Hong Kong, New Territories, Hong Kong

S *Supporting Information*

ABSTRACT: Ternary organic solar cells are emerging as a promising strategy to enhance device power conversion efficiency by broadening the range of light absorption via the incorporation of additional light-absorbing components. However, how to find compatible materials that allow comparable loadings of each component remains a challenge. In this article, we focus on studying the donor polymer compatibilities in ternary systems from a morphological point of view. Four typical donor polymers with different chemical structures and absorption ranges were mutually combined to form six distinct ternary systems with fullerene derivative acceptors. Two compatible ternary systems were identified as showing significant improvements of efficiency from both binary control devices. Ternary morphologies were characterized by grazing incident X-ray scattering and correlated with device performance. We find that polymers that have strong lamellar interactions and relatively similar phase separation behaviors with the fullerene derivative are more likely to be compatible in ternary systems. This result provides guidance for polymer selection for future ternary organic solar cell research while relaxing the limitation of chemical structure similarity and greatly extends the donor candidate pool.

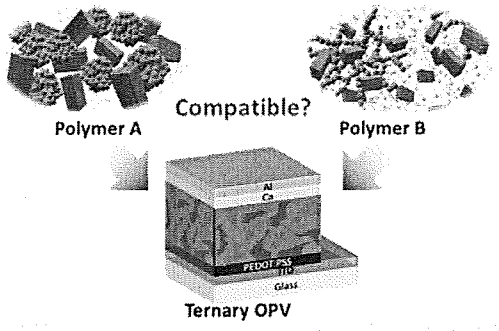

INTRODUCTION

Due to the appealing potential of producing low cost, flexible, multicolor, nontoxic, and lightweight photovoltaic devices, bulk heterojunction organic solar cells (OSCs) have attracted extensive research attention.[1,2] In a typical bulk heterojunction (BHJ) active layer, semiconducting polymers or small molecules act as the electron donor as well as the major light absorber while fullerene derivatives act as the electron acceptor. There are many routes to enhance the power conversion efficiency (PCE) of single-junction OSCs, including synthesizing new donor and acceptor materials,[3−5] optimizing active layer morphology,[6−8] interface engineering,[9,10] device structure engineering,[11,12] etc. Recently, the record PCE of single-junction cell has been pushed over 11%,[13] approaching the theoretical limit.[14] To bypass this limitation, employing more than one light absorbing donor or acceptor material becomes one of the promising solutions. In this regard, fabricating a tandem cell which incorporates multiple light absorbers via multiple junctions has attracted a lot of attention.[15−17] For instance, a triple tandem cell based on P3HT:ICBA, PTB:$PC_{71}BM$, and LBG:$PC_{71}BM$ successfully achieved a remarkably wide absorption range from 300 to 900 nm leading to a PCE of 11.5%.[18] However, tandem cells usually require very complicated fabrication processes for multilayer stacking which inevitably reduces the reproducibility and increases the fabrication cost.

On the other hand, ternary (or multinary) BHJ cells fabricated by simply mixing several light absorbing materials with complementary absorption spectra to form a single-junction cell can also expand the theoretical PCE limit at the same time as avoiding complicated processes experienced in tandem cell fabrication. The record PCE for ternary cells has been pushed to 10.5% recently.[19] However, challenges remain in fabricating ternary cells as well. How to choose compatible polymers, which are capable of working with similar loadings in BHJ, is one of the biggest issues. Studies have shown that many

Received: June 5, 2016
Revised: August 7, 2016
Published: August 8, 2016

 © 2016 American Chemical Society

DOI: 10.1021/acs.chemmater.6b02264
Chem. Mater. 2016, 28, 6186−6195

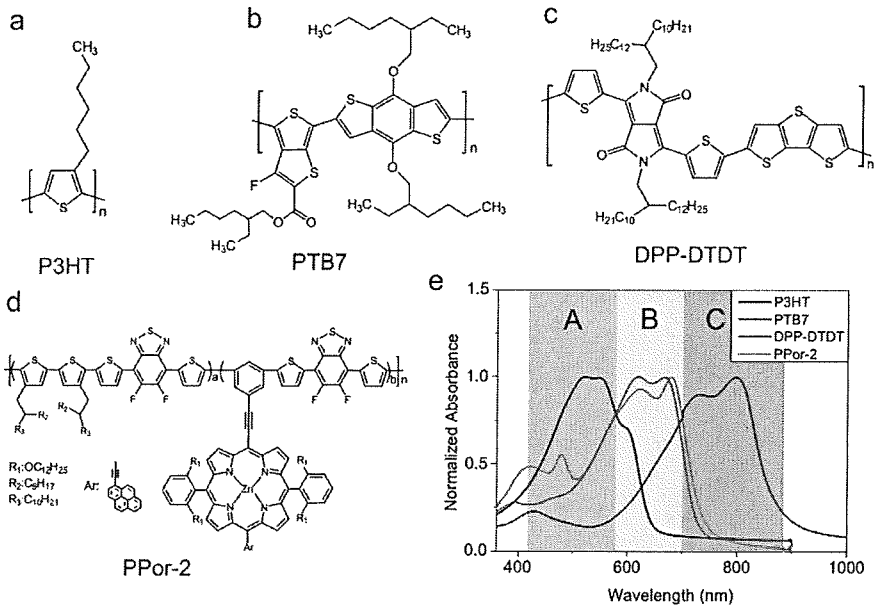

Figure 1. Chemical structures and absorption spectra. Chemical structures of (a) P3HT, (b) PTB7, (c) DPP-DTDT, and (d) PPor-2; (e) UV–vis absorption spectra of the four polymers.

polymer combinations cannot work with comparable loadings in ternary cells.[19−22] In the PBDTTT-EFT:PDVT-10:$PC_{71}BM$ system, device performance starts to decrease when the concentration of PDVT-10 exceeds 0.5%.[23] Chen reported that, with a small addition of bipolar poly[2,3-bis(thiophen-2-yl)-acrylonitrile-9,90-dioctyl-fluorene] (FLC8), the ternary (P3HT:FLC8:PCBM = 1:0.05:0.8) PCE has 30% increase compared with that of the P3HT:PCBM device due to the charge transfer improvement.[24] In these cases, the third component with much less concentration will contribute little to broadening the absorption range, preventing significant improvement in PCE. In some recently reported high PCE ternary systems, the optimized loadings of two absorbers are relatively comparable such as DTPyT:DTffBT = 1:1[25] and TAZ:DTBT = 3:7,[25] giving remarkable enhancement in light absorption and quantum efficiency (QE). Herein, people started to learn from successful systems the rule of choosing compatible polymers. Thompson studied the influence of polymer compatibility on the V_{oc} of the ternary solar cell, suggesting that similar surface energy and chemical structure facilitate the formation of polymer alloy which is beneficial to device performance.[26,27] Yang reported the structural, electronic, and photovoltaic characteristics of benzodithiophene based polymer ternary systems and concluded that, besides chemical structure similarity, similarities in molecular orientation, crystallite, and domain size are also important signatures of polymer compatibility.[28]

In this work, we relax the confinement of chemical structure similarity and investigate the general rules to select compatible polymers for ternary cells from a morphology point of view. We choose four typical polymers with completely different chemical structures. These four polymers were combined mutually to form six distinct ternary systems with [6,6]-phenyl C71-butyric acid methyl ester ($PC_{71}BM$). Despite of the lack of chemical structure similarity, we identified several highly compatible systems exhibiting excellent device performance. The ternary morphology is characterized by synchrotron based X-ray scattering techniques from the molecular scale to nanometer scale and correlated with its device performance. We found that the morphology compatibility in terms of molecular packing and phase separation is the key to donor polymer selection. To this end, the confinement on chemical structure similarity is totally relaxed which greatly extends the donor candidate pool for ternary organic solar cell research. Our results can be used as a guidance for prescreening and synthesizing compatible polymer groups for ternary solar cell fabrication.

EXPERIMENTAL SECTION

Materials. P3HT was purchased from Rieke Metals, PTB7 from Lumtech, and $PC_{71}BM$ from American Dye Source. DPP-DTDT was obtained from Dr. Jun Li, Imperial College London, and PPor-2 from Prof. Chain-shu Hsu, National Chiao Tung University. All these materials are used as received without any modification or purification.

Device Fabrication. All polymers and $PC_{71}BM$ were separately dissolved in ortho-dichlorobenzene (DCB) and mixed as binary solutions: P3HT:$PC_{71}BM$ (1:1) 40 mg/mL, PTB7:$PC_{71}BM$ (1:1.5) 40 mg/mL, DPP-DTDT:$PC_{71}BM$ (1:2) 20 mg/mL, and PPor-2:$PC_{71}BM$ (1:2) 40 mg/mL. Then binary solutions are mixed according to the designed polymer mass ratio to form ternary solar cells. The 3% diiodooctane addictive was added if the ternary solutions contain PTB7. ITO substrates were cleaned stepwise with deionized water, acetone, and isopropanol in ultrasonic cleaner for 20 min and then treated with oxygen plasma. The PEDOT:PSS layer was spun coated on the cleaned ITO substrates with a spin speed of 4000 rpm and then annealed under 130 °C for 20 min in a glovebox. Active layers were spun coated on the surface of PEDOT:PSS, and the thicknesses are controlled by spin speed. With the above binary solutions, ~110 nm active layers were achieved with 2500 rpm, and their ternary mixture solutions of different mass ratios could all achieve the similar thickness with the same spin speed. Solutions that contain DPP-DTDT should be heated under 65 °C before the spin coating because the viscosity of DPP-DTDT is very high in room temperature. After the active layers were dried in a nitrogen atmosphere for 30 min, methanol treatment[9] was performed. Next, 10 nm Ca and 100 nm Al are evaporated onto the active layer under a vacuum of 7×10^{-4} Pa.

Characterization Method. The solar cell performance was measured by a Keithley 2612 source meter unit under an AM 1.5G

DOI: 10.1021/acs.chemmater.6b02264
Chem. Mater. 2016, 28, 6186−6195

Table 1. Polymer Properties and Combinations

	polymer			
	P3HT	PTB7	DPP-DTDT	PPor-2
absorption range	A	B	C	B
crystallinity	high	low	medium	medium
orientation	edge-on	face-on	edge-on	edge-on

group no. 1: P3HT:PTB7:$PC_{71}BM$ group no. 2: P3HT:DPP-DTDT:$PC_{71}BM$ group no. 3: P3HT:PPor-2:$PC_{71}BM$
group no. 4: PTB7:DPP-DTDT:$PC_{71}BM$ group no. 5: PTB7:PPor-2:$PC_{71}BM$ group no. 6: DPP-DTDT:PPor-2:$PC_{71}BM$

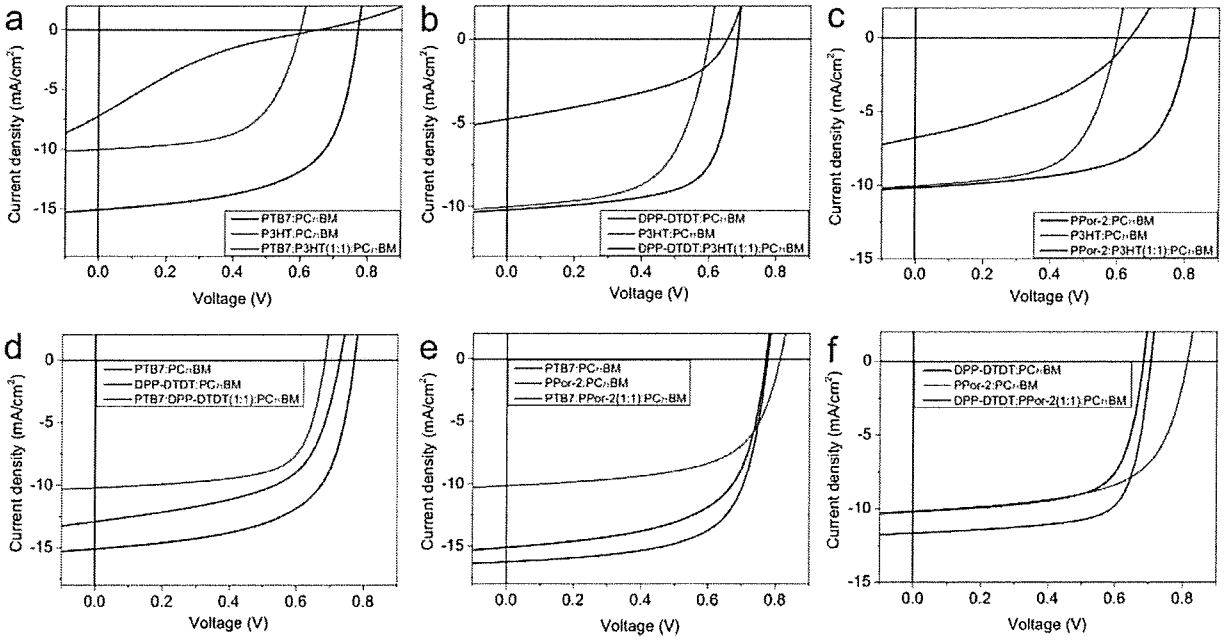

Figure 2. *J–V* curves of ternary solar cells and their binary control cells. (a) Group no. 1 (P3HT:PTB7:$PC_{71}BM$), (b) group no. 2 (P3HT:DPP-DTDT:$PC_{71}BM$), (c) group no. 3 (P3HT:PPor-2:PC71BM), (d) group no. 4 (DPP-DTDT:PTB7:$PC_{71}BM$), (e) group no. 5 (PTB7:PPor-2:$PC_{71}BM$), and (f) group no. 6 (DPP-DTDT:PPor-2:$PC_{71}BM$). All ternary solar cells have polymer mass ratio of 1:1.

solar simulator with an intensity of 100 mW/cm^2. UV–vis absorption spectra were taken on a Cary 5G UV–vis–NIR spectrophotometer.

The GIWAXS measurements were conducted at 23A SWAXS beamline at the National Synchrotron Radiation Research Center, Hsinchu, Taiwan, using a 10 keV primary beam, 0.15° incident angle, and Pilatus 1M-F and C9728DK area detector.[29] GISAXS measurement is conducted at 16B SAXS beamline at Shanghai Synchrotron Radiation Facility, Shanghai, China, also using the 0.15° incident angle with 10 keV primary beam. Both GIWAXS and GISAXS samples are prepared on PEDOT:PSS coated silicon substrate by spin coating.

RESULTS AND DISCUSSION

Materials Selection. The four polymers chosen for this study are poly(3-hexylthiophene-2,5-diyl) (P3HT), poly({4,8-bis[(2-ethylhexyl)oxy]benzo[1,2-b:4,5-b′]dithiophene-2,6-diyl}{3-fluoro-2-[(2-ethylhexyl)carbonyl]thieno[3,4-*b*]-thiophenediyl}) (PTB7), poly(5,6-difluoro benzothiadiazole-*alt*-quaterthiophene) containing porphyrin side groups (PPor-2), and poly[(2,5-{2-decyl-tetradecyl}-3,6-diketopyrrolopyrrole)-*alt*-5,5-(2′,6′-dithiophen-2-yl-dithieno[3,2-b;2′,3′-d]-thiophene)] (DPP-DTDT). Figure 1a–d summarizes their chemical structures. Here, P3HT is the most studied prototypical donor polymer that exhibits stable device performance and is commercially available.[30] PTB7 is a well-known low-bandgap polymer with high performance, also commercially available.[3] PPor-2 is a porphyrin-incorporated two-dimensional donor–acceptor polymer with similar bandgap as PTB7.[31] DPP-DTDT is also a low-bandgap polymer based on a backbone of diketopyrrolo–pyrrole–dithiophene–thienothiophene prepared by a method similar to that reported previously for DPP-DTT.[32,33] In order to diversify our samples, the four polymer donors have not only different chemical structures but also different absorption ranges, polymer crystallinities, and orientations. Figure 1e summarizes their absorption spectra. P3HT has a relatively large bandgap, and thereby its absorption edge locates at a shorter wavelength (~650 nm). The absorption edges of PTB7 and PPor-2 are similar, around 730 nm. DPP-DTDT has the smallest bandgap among these four polymers with an absorption edge around 900 nm. The pure polymer crystallinity and molecule orientation were investigated by grazing incident wide-angle X-ray scattering (GIWAXS) measurements and are presented in Figure S1. P3HT shows a high intensity of lamellar peaks along the q_z axis, consistent with its well-known high crystallinity and edge-on structure. PTB7 exhibits a relatively low intensity of lamellar peak along the q_x axis indicative of its preferential face-on orientation and relatively low crystallinity. Both DPP-DTDT and PPor-2 have edge-on orientation and medium crystallinity between that of P3HT and that of PTB7. With these four polymers covering different absorption ranges, crystallinities,

DOI: 10.1021/acs.chemmater.6b02264
Chem. Mater. 2016, 28, 6186–6195

Table 2. Photovoltaic Device Characteristics[a]

sample	PCE (%)	FF	J_{sc} (mA/cm^2)	V_{oc} (V)
P3HT:$PC_{71}BM$	3.1 ± 0.2	0.58 ± 0.01	8.9 ± 0.4	0.60 ± 0.01
PTB7:$PC_{71}BM$	7.1 ± 0.2	0.61 ± 0.01	15.3 ± 0.4	0.77 ± 0.01
DPP-DTDT:$PC_{71}BM$	4.9 ± 0.1	0.69 ± 0.01	10.5 ± 0.2	0.68 ± 0.01
PPor-2:PC71BM	5.0 ± 0.1	0.61 ± 0.01	10.1 ± 0.3	0.81 ± 0.01
no. 1: P3HT:PTB7(1:1):$PC_{71}BM$	0.9 ± 0.1	0.23 ± 0.02	5.8 ± 0.3	0.67 ± 0.01
no. 2: P3HT:DPP-DTDT(1:1):$PC_{71}BM$	1.2 ± 0.1	0.40 ± 0.02	4.8 ± 0.5	0.62 ± 0.01
no. 3: P3HT:PPor-2(1:1):$PC_{71}BM$	0.4 ± 0.1	0.28 ± 0.03	2.3 ± 0.3	0.65 ± 0.01
no. 4: PTB7:DPP-DTDT(1:1):$PC_{71}BM$	5.3 ± 0.1	0.59 ± 0.01	12.5 ± 0.1	0.73 ± 0.01
no. 5: PTB7:PPor-2(1:1):$PC_{71}BM$	8.2 ± 0.1	0.65 ± 0.01	16.2 ± 0.4	0.78 ± 0.01
no. 6: DPP-DTDT:PPor-2(1:1):$PC_{71}BM$	6.0 ± 0.2	0.72 ± 0.01	11.7 ± 0.3	0.70 ± 0.01

[a]Each value is averaged from 12 devices with standard deviation after ±.

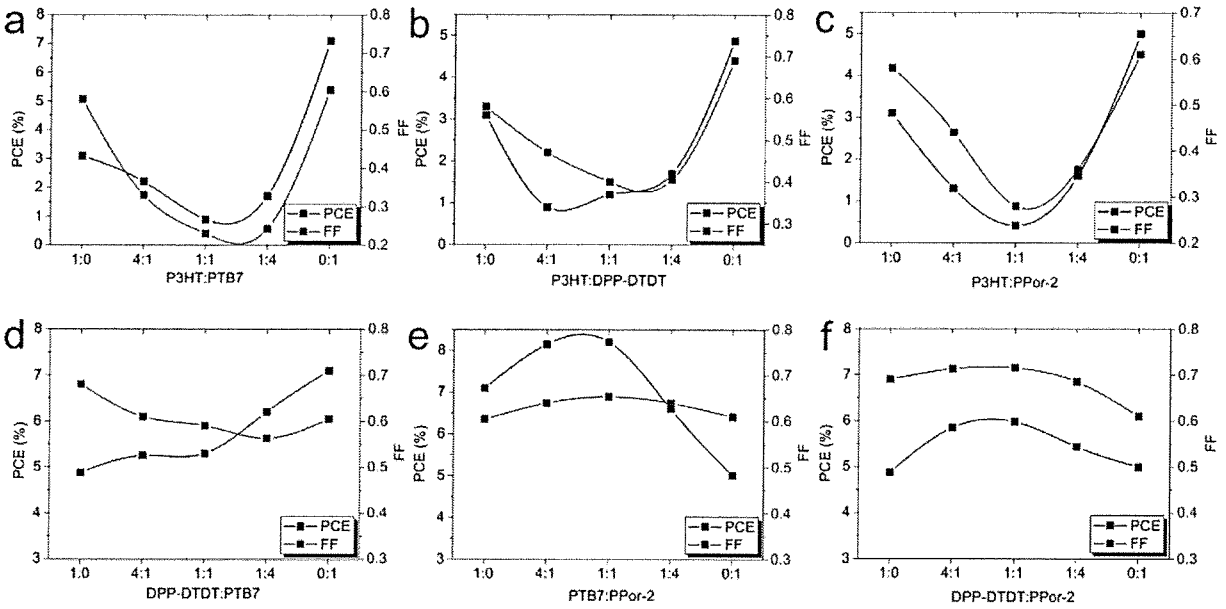

Figure 3. PCEs and FFs of ternary solar cells as a function of mass ratio of polymers for the six ternary groups. (a) Group no. 1 (P3HT:PTB7:$PC_{71}BM$), (b) group no. 2 (P3HT:DPP-DTDT:$PC_{71}BM$), (c) group no. 3 (P3HT:PPor-2:PC71BM), (d) group no. 4 (DPP-DTDT:PTB7:$PC_{71}BM$), (e) group no. 5 (PTB7:PPor-2: $PC_{71}BM$), (f) group no. 6 (DPP-DTDT:PPor-2:$PC_{71}BM$). (The values are averaged from 12 devices).

and molecule orientations, we have six diversified groups of ternary systems, as summarized in Table 1.

Photovoltaic Device Characterization. To identify whether the polymers are compatible, photovoltaic devices based on the six ternary groups and their binary controls have been fabricated with a conventional device structure of ITO/PEDOT:PSS/active layer/Ca/Al. For simple comparison, the mass ratio of the two donor polymers was kept at 1:1, which might not be the optimum mass ratio for best device performance but fair enough to demonstrate the polymer compatibility. The loading of $PC_{71}BM$ in the ternary cell was kept to the summation of optimized $PC_{71}BM$ loadings in the binary cells. Figure 2 shows $J-V$ curves of the six groups, and Table 2 summarizes the corresponding device characteristics. Obviously, group nos. 5 (PTB7:PPor-2:$PC_{71}BM$) and 6 (DPP-DTDT:PPor-2:$PC_{71}BM$) have demonstrated much better PCEs with ternary BHJ (8.2% and 6.0%, respectively) than the corresponding binary controls (no. 5: 7.1% and 5.0%; no. 6: 4.9% and 5.0%), indicating good compatibilities of these two groups. On the other hand, the ternary cell made of PTB7:DPP-DTDT:$PC_{71}BM$ (no. 4) exhibited medium performance lying between the performance of both binary cells. It implies that the compatibility of DPP-DTDT/PTB7 (no. 4) is not as good as that of DPP-DTDT/PPor-2 (no. 6) and PTB7/PPor-2 (no. 5), which means that the polymer compatibility is not transitive. The ternary cells with P3HT as one of the components (group nos. 1–3) have shown drastic deterioration in device performance, suggesting that P3HT is compatible with none of the rest of the three polymers. In summary, the compatibility of the selected six ternary groups can be ranked in terms of relative device performance compared with their binary controls, as follows:

$$\text{Group nos. 1, 2, 3} < \text{Group no. 4} < \text{Group nos. 5, 6} \quad (1)$$

The device results have provided strong evidence that chemical structure similarity is not a necessity for polymers to be compatible in ternary cells. It is also worth noting that the PCE improvements are not merely contributed from the increase of short circuit current (J_{sc}) but also fill factor (FF). In fact, the absorption spectra of PTB7 and PPor-2 are largely

DOI: 10.1021/acs.chemmater.6b02264
Chem. Mater. 2016, 28, 6186–6195

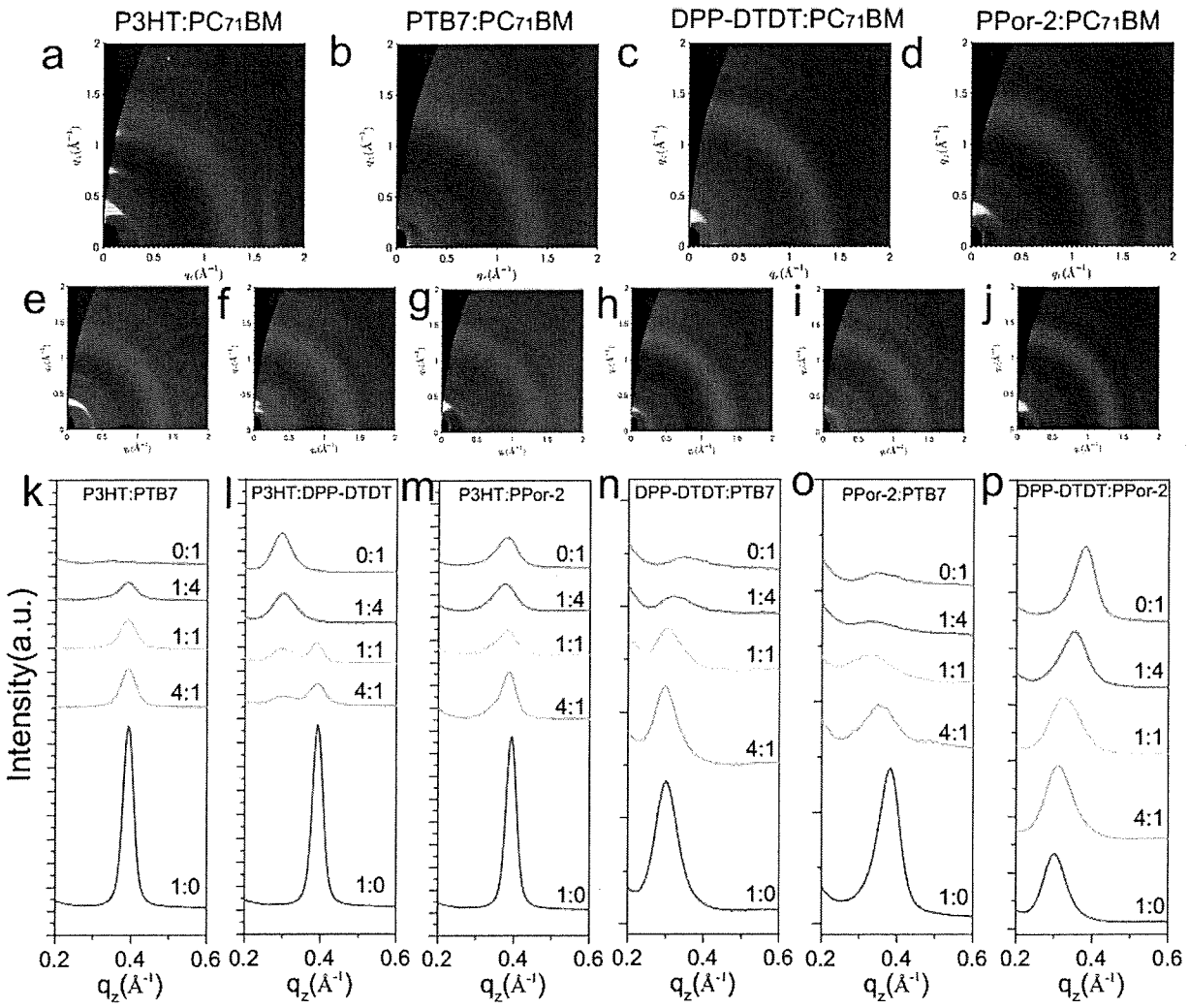

Figure 4. GIWAXS patterns and intensity profiles. GIWAXS patterns of binary films (a) P3HT:$PC_{71}BM$, (b) PTB7:$PC_{71}BM$, (c) DPP-DTDT:$PC_{71}BM$, and (d) PPor-2:$PC_{71}BM$; and ternary films (e) group no. 1 (P3HT:PTB7:$PC_{71}BM$), (f) group no. 2 (P3HT:DPP-DTDT:$PC_{71}BM$), (g) group no. 3 (P3HT:PPor-2:PC71BM), (h) group no. 4 (DPP-DTDT:PTB7:$PC_{71}BM$), (i) group no. 5 (PTB7:PPor-2:$PC_{71}BM$), (j) group no. 6 (DPP-DTDT:PPor-2:$PC_{71}BM$), and (k–p) the corresponding intensity profiles along the q_z axis.

overlapping (Figure 1e). Both ternary groups no. 5 and no. 6 can maintain remarkably high FF. Especially for group no. 6, FFs are consistently larger than 65% with different mass ratios of polymers (Figure 3f). It suggests that other reasons beyond absorption range extension should be taken into account for the device improvements of ternary cells.

Morphology Characterization. For solution-processed organic BHJ solar cells, the morphology of the active layer is known to be critical to the device performance.[34−36] In a ternary system, the addition of another component for sure increases the complexity of morphology. Many previous studies have demonstrated significant influences of the third component as an additive on morphology and device performance.[37,38] For instance, 1 wt % of P3HT was reported to induce favorable domain size and phase separation in the PCPDTBT/$PC_{61}BM$ system, leading to 20% improvement in PCE.[39] Thus, for our case with much larger amount of the third component, systematic study of morphology is needed. To characterize the film morphology, we employ grazing-incidence wide-angle and small-angle X-ray scattering (GIWAXS and GISAXS) techniques to extract structural information from molecular scale to nanostructure scale: GIWAXS is used to characterize the molecular packing information such as polymer crystallinity and molecular orientation while GISAXS is able to unveil nanoscale phase separation information.[22,40−42]

Figure 4a–d presents the GIWAXS patterns of binary films made of each selected polymer blended with $PC_{71}BM$. Similar to previous reports,[41] the P3HT:$PC_{71}BM$ film (Figure 4a) exhibited the highest crystallinity and edge-on order, showing up to three orders of lamellar peaks with (100) located at q_z = 0.39 $Å^{-1}$ (d = 16 Å) and a (010) π–π peak at q_r = 1.65 $Å^{-1}$ (d = 3.8 Å) . According to Scherrer's equation,[43] the coherence length was ~160 Å for P3HT lamellar stacking, estimated by $L = 2\pi/\Delta q$, where Δq is the full width at half-maximum of the lamellar peak. The PTB7:$PC_{71}BM$ film (Figure 4b) is more amorphous than the pure PTB7 film (Figure S1b), showing a weak and broad lamellar ring centered at q = 0.33 $Å^{-1}$ (d = 19 Å) and an estimated coherence length of ~49 Å. The DPP-

DOI: 10.1021/acs.chemmater.6b02264
Chem. Mater. 2016, 28, 6186−6195

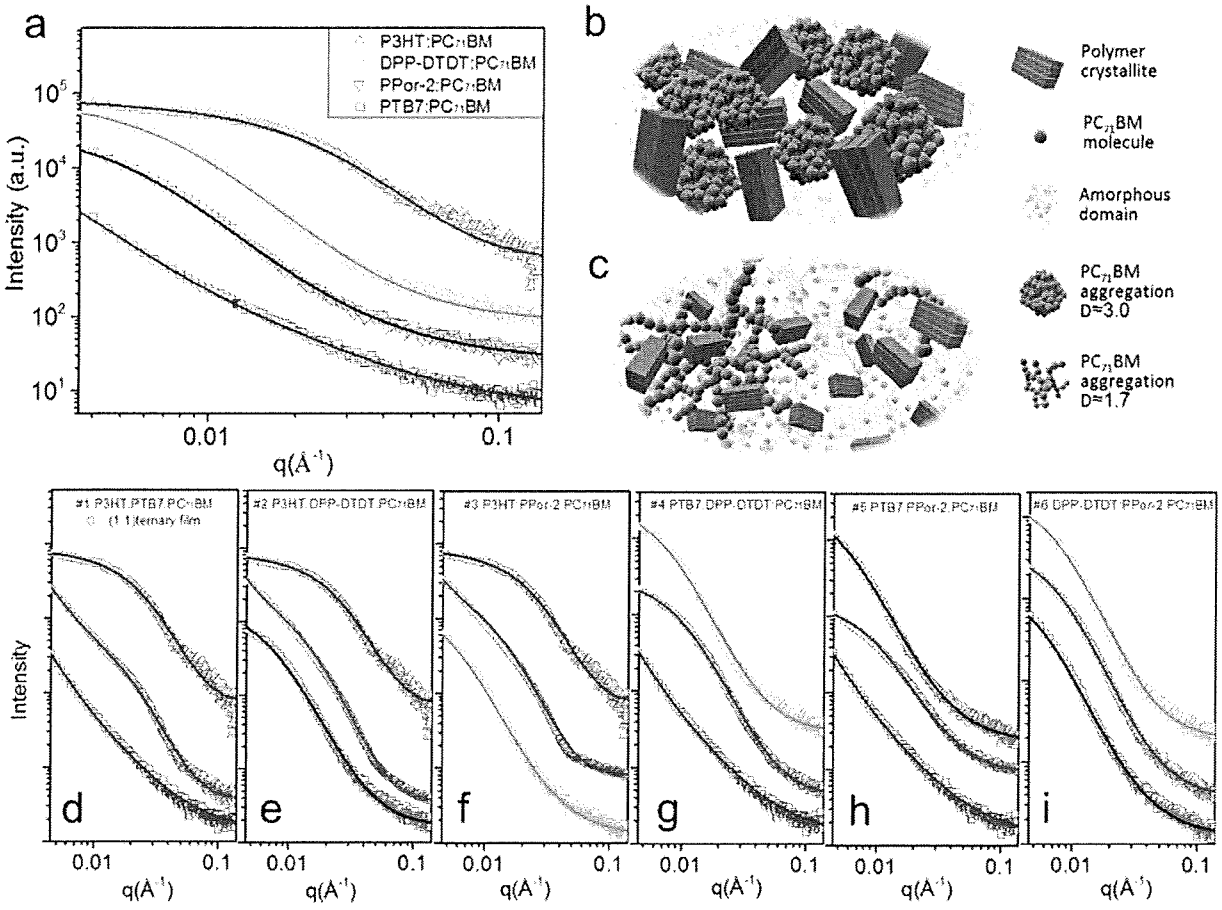

Figure 5. GISAXS profiles and schematics of BHJ morphology. (a) GISAXS profiles of the four binary films and their model fittings (solid line); (b, c) schematic diagrams of BHJ morphology with $PC_{71}BM$ aggregation fractal dimension of 3 and 1.7, respectively; (e–j) GISAXS profiles of (1:1) ternary films (purple) and their binary controls for the six groups.

DTDT:$PC_{71}BM$ film (Figure 4c) shows a (100) lamellar peak at q_z = 0.30 Å^{-1} (d = 21 Å) and a coherence length of ~95 Å, demonstrating moderate crystallinity as well as edge-on order. Similarly, for PPor-2:$PC_{71}BM$ film (Figure 4d), we observed a (100) lamellar peak at q_z = 0.38 Å^{-1} (d = 17 Å, L = ~96 Å) and a (010) π–π peak at q_r = 1.78 Å^{-1} (d = 3.5 Å), indicating preferential edge-on orientation of polymer domains.

The GIWAXS patterns of the six ternary films are shown in Figure 4e–j. The corresponding intensity profiles along the q_z axis in the vicinity of (100) lamellar peaks are presented in Figure 4k–p. The molecular packing distance for P3HT domains are hardly disturbed when mixing with another polymer, as evidenced by the appearance of the P3HT (100) lamellar peak at q_z = 0.39 Å^{-1} for all the films with P3HT (Figure 4e–g). The overall film crystallinity is decreased as indicated by the weakening of scattering intensity, which is commonly observed for many ternary systems.[44] For the P3HT:PTB7:$PC_{71}BM$ film (Figure 4e), the PTB7 phase stays amorphous since no obvious PTB7 lamellar peak was observed. For the P3HT:DPP-DTDT:$PC_{71}BM$ film, we observed obvious double peaks at q_z = 0.39 and 0.30 Å^{-1} (Figure 4f), which can be assigned to P3HT and DPP-DTDT lamellar stacking, respectively. This implies that the molecular packing of DPP-DTDT is also preserved in the ternary film with P3HT. For the P3HT:PPor-2:$PC_{71}BM$ film, we did not observe similar lamellar peak splitting as observed in the P3HT:DPP-DTDT:$PC_{71}BM$ film, due to the close lamellar packing distance of P3HT (16.1 Å) and PPor-2 (16.5 Å).

The molecular packing behaviors of the relatively compatible group nos. 4–6 (PTB7:PPor-2:$PC_{71}BM$, DPP-DTDT:PTB7:$PC_{71}BM$, and DPP-DTDT:PPor-2:$PC_{71}BM$) films (Figure 4h–j) are quite different from those of the incompatible groups. Only one lamellar peak was observed for all the cases, and the peak position moves with the same trend as the mass ratio of the two polymers changes. This is an interesting finding that we do not fully understand yet. It is possible that the polymers still pack in their own phases while the lamellar distances tend to change to closer values due to conjugated π–π interaction. It could be also due to the highly mixing of the two polymer phases so that the molecular packing of the two polymers is intertwined with each other, forming "organic alloys", which was proposed in several previous studies.[27,45,46] The surface free energy measured for the four polymers (Table S1) shows similar behavior observed in refs 27 and 46 that smaller surface energy difference, which is considered a sign of better polymer miscibility, corresponds to better compatibility, in support of the alloy model. In these studies,[27,45,46] a monotonic evolution of V_{oc} with composition was also observed as a strong evidence of alloy formation. However, for our cases, we only find such a phenomenon in

DOI: 10.1021/acs.chemmater.6b02264
Chem. Mater. 2016, 28, 6186–6195

Table 3. Fitting Parameters of Binary and (1:1) Ternary Films, Where ξ, $2R_{gPC71BM}$, and D Are Obtained from GISAXS Fitting and $L_{polymer}$ Is the Coherence Length Obtained from GIWAXS Data

sample	ξ (Å)	$2R_{gPC71BM}$ (Å)	D	$L_{polymer}$ (Å)
P3HT:$PC_{71}BM$	172	193	2.97	162
DPP-DTDT:$PC_{71}BM$	129	531	1.96	95
PPor-2:$PC_{71}BM$	179	596	1.87	96
PTB7:$PC_{71}BM$	456	1036	1.75	49
P3HT:PTB7(1:1):$PC_{71}BM$	411	281	2.97	N/A
P3HT:DPP-DTDT(1:1):$PC_{71}BM$	359	359	2.97	N/A
P3HT:PPor-2(1:1):$PC_{71}BM$	361	350	2.98	N/A
PTB7:DPP-DTDT(1:1):$PC_{71}BM$	98	574	2.29	N/A
PTB7:PPor-2(1:1):$PC_{71}BM$	90	518	2.01	N/A
DPP-DTDT:PPor-2(1:1):$PC_{71}BM$	125	575	1.96	N/A

group no. 4 and no. 6 but not no. 5 (Figure S3). On the other hand, the composition-dependent V_{oc} is also observed in noncompatible group no. 1 and no. 3 (Figure S3). A systematic work on more polymers that will provide better understanding of this point is, however, beyond the scope of this manuscript. We speculate that the unifying of polymer lamellar packing distances could enhance the internal order of polymer domains and facilitate charge transport, which would contribute to the observed compatible ternary device performance based on these combinations (Table 2). It is worth noting that PTB7 is known to be preferentially face-on oriented,[47] which is favorable for vertical charge transport in photovoltaic devices.[48,49] This advantage is weakened after mixing with $PC_{71}BM$ as indicated by the disappearance of the face-on $\pi-\pi$ peak along the q_z axis (Figure 4b). Remarkably, the face-on $\pi-\pi$ peak becomes more prominent in PTB7:PPor-2:$PC_{71}BM$ (no. 5) ternary films (Figure 4i), suggesting that the mixing of compatible polymers could also promote $\pi-\pi$ stacking.

GISAXS intensity profiles of binary films are presented in Figure 5a, which provide information about nanoscale phase separation behavior in the BHJ films. The corresponding two-dimensional GISAXS patterns are shown in Figure S2. The intensity profiles are extracted at the reflected beam position (incident angle = 0.15°) along the q_r axis for enhanced signals.[41] The GISAXS profile of the P3HT:$PC_{71}BM$ film exhibits an obvious shoulder at q = ~0.03 $Å^{-1}$, implying the presence of structure order of ~200 Å. This is often interpreted as the effect of strong P3HT: $PC_{71}BM$ phase separation where the scattering of aggregated $PC_{71}BM$ clusters gives rise to the observed shoulder.[41] For DPP-DTDT:$PC_{71}BM$ and PPor-2:$PC_{71}BM$, the shoulder is not as prominent as that presented in P3HT:$PC_{71}BM$ and moves to lower q region around 0.01 $Å^{-1}$ corresponding to a relatively larger length-scale structure order of ~600 Å. For the PTB7:$PC_{71}BM$ film, no obvious shoulder was observed, which is consistent with the amorphous nature of the PTB7:$PC_{71}BM$ film.

To quantify and compare the phase separation behaviors of different polymers with $PC_{71}BM$, we have fitted all the GISAXS profiles with a universal model:

$$I(q) = \frac{A_1}{[1 + (q\xi)^2]^2} + A_2\langle P(q, R)\rangle S(q, R, \eta, D) + B \quad (2)$$

where the first term was the so-called Debye–Anderson–Brumberger (DAB) term,[50] modeling the scattering from dispersed $PC_{71}BM$ molecules within amorphous polymer domains where q is the scattering wave vector, A_1 is an independent fitting parameter, and ξ is the average correlation length of the amorphous domain. The second term represents the contribution from clustered $PC_{71}BM$. Here, $P(q, R)$ is the form factor of $PC_{71}BM$ modeled as spheres with mean radius of R = 5 Å. $S(q, R, \eta, D)$ is the structure factor of clustered $PC_{71}BM$ domains modeled as fractal-like networks,[51,52] which can be expressed as

$$S(q) = 1 + \frac{\sin[(D-1)\tan^{-1}(q\eta)]}{(qR)^D}\frac{D\Gamma(D-1)}{\left[1 + \frac{1}{(q\eta)^2}\right]^{(D-1)/2}} \quad (3)$$

where R is again the mean spherical radius of $PC_{71}BM$, η is the correlation length of the fractal-like network, and D is the fractal dimension of the structure. The average domain size of the clustered fullerene phases is approximately characterized by the Guinier radius of the fractal-like network R_g where $R_g = \left(\frac{D(D+1)}{2}\right)^{1/2}\eta$. In this model, the scattering contributions from crystalline polymer domains are ignored since no significant aggregation of these domains was observed to produce enough contrast with the amorphous polymer background.

The average sizes of the crystalline polymer domain, amorphous polymer domain, and clustered $PC_{71}BM$ domains can be roughly estimated by GIWAXS fitting results of coherence length $L_{polymer}$ and GISAXS fitting results of ξ and $2R_{gPC71BM}$, which are summarized in Table 3. For binary films from the top (P3HT) to the bottom (PTB7), the size of crystalline polymer domains ($L_{polymer}$) decreases due to the gradual decrease of polymer crystallinity observed in GIWAXS. For clustered $PC_{71}BM$ domains, it is intriguing that the fractal size ($2R_{gPC71BM}$) increases along with the decrease of the fractal dimension (D) for binary films. Intuitively, smaller fractal dimension corresponds to less space filling, in other words, more loosely packed aggregation.[53,54] Figure 5b,c illustrates the schematic phase separation behavior with clustered $PC_{71}BM$ fractal dimensions around 3.0 and 1.7, respectively. With a fractal dimension of ~3.0, the $PC_{71}BM$ clusters are nearly close-packed solid. When the fractal dimension decreases to 1.7, $PC_{71}BM$ molecules form much more loosely packed fractal networks but extend to larger regions facilitating both exciton dissociation and charge transport. This scenario well explains the reason for excellent device performance of PTB7 in spite of relatively amorphous morphology. It is interesting to find that better polymer compatibility correlates with closer values of fractal dimension in binary films. For instance, the fractal dimension differences are much smaller for compatible polymers (no. 5: 1.96−1.87 = 0.09, no. 6: 1.87−1.75 = 0.12,

DOI: 10.1021/acs.chemmater.6b02264
Chem. Mater. 2016, 28, 6186−6195

and no. 4: 1.96−1.75 = 0.19) than the incompatible groups (no. 1: 2.97−1.96 = 1.01, no. 2: 2.97−1.87 = 1.1, and no. 3: 2.97−1.75 = 1.22), which indicates that similar $PC_{71}BM$ cluster packing densities in binary film might be another important signature of compatibility.

The GISAXS profiles of ternary films are presented in Figure 5d−i with the fitting parameters also shown in Table 3. Ternary morphology is much more complicated than binary morphology. The addition of one more component could introduce several new phases such as pure amorphous and crystalline phases for the third polymer, its phases intermixing with the other two components. However, we did not observe large aggregation of polymer crystalline phases, and there is not much electron density contrast between polymers; in other words, the two polymers are indistinguishable in GISAXS. Thereby, we still treat the ternary system as a binary polymer:fullerene system and use the same model to fit the GISAXS profiles. From the GISAXS fitting results of ternary films (Table 3), we found that incompatible ternary groups (nos. 1−3) have much larger amorphous phase, consistent with the crystallinity decrease observed in GIWAXS. In contrast, the amorphous domain size remains unchanged or even shrinks for compatible groups (nos. 4−6), probably due to the cocrystallization ability of compatible polymers. This also supports the unifying of the lamellar stacking distance observed in GIWAXS of compatible groups.

Using the same solvent and processing procedure, the formation of BHJ morphology is known to be a spontaneous process leading to the lowest energy state largely determined by the interaction between polymer and fullerene.[55] It is the intrinsic property of a polymer to form a certain morphology with fullerene, which is related to their interface potential. When selecting polymer candidates for ternary devices, it is natural to choose from those already demonstrating good performance. Thereby, the binary morphology is presumably a good morphology. When mixing as a ternary BHJ, a fullerene framework that is in favor of both polymers is a reasonable requirement for good performance. It suggests by our results that two polymers that have similar frameworks of the $PC_{71}BM$ phase in a binary film are able to maintain their $PC_{71}BM$ morphology in their ternary film, resulting in high compatibility in performance.

CONCLUSIONS

In summary, we selected four polymers with completely different chemical structures and properties. We studied their mutual compatibility when making ternary BHJ solar cells with $PC_{71}BM$. Among the six ternary systems studied, three groups showed the worst performance, one group showed medium performance, and two groups showed much better device performance than their binary controls.

Grazing-incidence X-ray scattering results provide us several insights on judging the morphology compatibility of polymers. First, in terms of molecular packing, high polymer−polymer interaction signified by unified lamellar distances, enhanced $\pi-\pi$ stacking order, and shrinking of amorphous domain size after mixing can assist us to sort out compatible groups. Second, in terms of phase separation, our results suggest that similar fullerene packing density in binary cells could be another important signature. When forming a ternary BHJ, a fullerene framework that is favorable for both polymers is a reasonable requirement for compatible morphology and good performance. Thus, the initially similar $PC_{71}BM$ packing density in binary cells, which can be quantitatively described as a closer fractal dimension, could be a prerequisite when selecting candidate polymers for ternary cells.

Our results are not against the previous conclusions that polymers with similar chemical structures have better compatibility.[27,28] Indeed, polymers with similar chemical structures usually have similar morphologies and thereby are intrinsically compatible. Our conclusion relaxes this limitation and greatly extends the donor candidate pool for future ternary organic solar cell research.

ASSOCIATED CONTENT

Supporting Information

The Supporting Information is available free of charge on the ACS Publications website at DOI: 10.1021/acs.chemmater.6b02264.

GIWAXS patterns of the four polymers; GISAXS patterns of the binary films of the four polymer; the V_{oc} of ternary solar cells against mass ratio of polymers for all six ternary groups; surface free energy of four polymers and $PC_{71}BM$ (PDF)

AUTHOR INFORMATION

Corresponding Author

*(X.L.) E-mail: xhlu@phy.cuhk.edu.hk.

Notes

The authors declare no competing financial interest.

ACKNOWLEDGMENTS

We are grateful for the beam time and technical supports provided by 23A SWAXS beamline at NSRRC, Hsinchu, and BL14B1 and 16B1 beamlines at SSRF, Shanghai. We acknowledge the financial support from Research Grant Council of Hong Kong (General Research Fund No. 14303314, Theme-based Research Scheme No. T23-407/13-N, and CUHK Focused Innovation Scheme B No. 1902034).

REFERENCES

(1) Dennler, G.; Scharber, M. C.; Brabec, C. J. Polymer-Fullerene Bulk-Heterojunction Solar Cells. *Adv. Mater.* **2009**, *21* (13), 1323−1338.

(2) Blom, P. W. M.; Mihailetchi, V. D.; Koster, L. J. A.; Markov, D. E. Device Physics of Polymer:Fullerene Bulk Heterojunction Solar Cells. *Adv. Mater.* **2007**, *19* (12), 1551−1566.

(3) Liang, Y.; Xu, Z.; Xia, J.; Tsai, S. T.; Wu, Y.; Li, G.; Ray, C.; Yu, L. For the bright future-bulk heterojunction polymer solar cells with power conversion efficiency of 7.4%. *Adv. Mater.* **2010**, *22* (20), E135−E138.

(4) Liu, Y.; Zhao, J.; Li, Z.; Mu, C.; Ma, W.; Hu, H.; Jiang, K.; Lin, H.; Ade, H.; Yan, H. Aggregation and morphology control enables multiple cases of high-efficiency polymer solar cells. *Nat. Commun.* **2014**, *5*, 5293.

(5) Lin, Y.; He, Q.; Zhao, F.; Huo, L.; Mai, J.; Lu, X.; Su, C. J.; Li, T.; Wang, J.; Zhu, J.; Sun, Y.; Wang, C.; Zhan, X. A Facile Planar Fused-Ring Electron Acceptor for As-Cast Polymer Solar Cells with 8.71% Efficiency. *J. Am. Chem. Soc.* **2016**, *138* (9), 2973−2976.

(6) Hedley, G. J.; Ward, A. J.; Alekseev, A.; Howells, C. T.; Martins, E. R.; Serrano, L. A.; Cooke, G.; Ruseckas, A.; Samuel, I. D. Determining the optimum morphology in high-performance polymer-fullerene organic photovoltaic cells. *Nat. Commun.* **2013**, *4*, 2867.

(7) Lou, S. J.; Szarko, J. M.; Xu, T.; Yu, L.; Marks, T. J.; Chen, L. X. Effects of additives on the morphology of solution phase aggregates formed by active layer components of high-efficiency organic solar cells. *J. Am. Chem. Soc.* **2011**, *133* (51), 20661−20663.

DOI: 10.1021/acs.chemmater.6b02264
Chem. Mater. 2016, 28, 6186−6195

(8) Verploegen, E.; Mondal, R.; Bettinger, C. J.; Sok, S.; Toney, M. F.; Bao, Z. Effects of Thermal Annealing Upon the Morphology of Polymer-Fullerene Blends. *Adv. Funct. Mater.* **2010**, *20* (20), 3519–3529.
(9) Zhou, H.; Zhang, Y.; Seifter, J.; Collins, S. D.; Luo, C.; Bazan, G. C.; Nguyen, T. Q.; Heeger, A. J. High-efficiency polymer solar cells enhanced by solvent treatment. *Adv. Mater.* **2013**, *25* (11), 1646–1652.
(10) Alemu, D.; Wei, H.-Y.; Ho, K.-C.; Chu, C.-W. Highly conductive PEDOT:PSS electrode by simple film treatment with methanol for ITO-free polymer solar cells. *Energy Environ. Sci.* **2012**, *5* (11), 9662–9671.
(11) Lu, X.; Hlaing, H.; Nam, C.-Y.; Yager, K. G.; Black, C. T.; Ocko, B. M. Molecular Orientation and Performance of Nanoimprinted Polymer-Based Blend Thin Film Solar Cells. *Chem. Mater.* **2015**, *27* (1), 60–66.
(12) He, Z. C.; Zhong, C. M.; Su, S. J.; Xu, M.; Wu, H. B.; Cao, Y. Enhanced power-conversion efficiency in polymer solar cells using an inverted device structure. *Nat. Photonics* **2012**, *6* (9), 591–595.
(13) Zhao, J.; Li, Y.; Yang, G.; Jiang, K.; Lin, H.; Ade, H.; Ma, W.; Yan, H. Efficient organic solar cells processed from hydrocarbon solvents. *Nat. Energy* **2016**, *1* (2), 15027.
(14) Coakley, K. M.; McGehee, M. D. Conjugated polymer photovoltaic cells. *Chem. Mater.* **2004**, *16* (23), 4533–4542.
(15) Ameri, T.; Li, N.; Brabec, C. J. Highly efficient organic tandem solar cells: a follow up review. *Energy Environ. Sci.* **2013**, *6* (8), 2390–2413.
(16) Zhou, H.; Zhang, Y.; Mai, C. K.; Collins, S. D.; Bazan, G. C.; Nguyen, T. Q.; Heeger, A. J. Polymer homo-tandem solar cells with best efficiency of 11.3%. *Adv. Mater.* **2015**, *27* (10), 1767–1773.
(17) You, J.; Dou, L.; Hong, Z.; Li, G.; Yang, Y. Recent trends in polymer tandem solar cells research. *Prog. Polym. Sci.* **2013**, *38* (12), 1909–1928.
(18) Chen, C. C.; Chang, W. H.; Yoshimura, K.; Ohya, K.; You, J.; Gao, J.; Hong, Z.; Yang, Y. An efficient triple-junction polymer solar cell having a power conversion efficiency exceeding 11%. *Adv. Mater.* **2014**, *26* (32), 5670–5677.
(19) Zhang, J.; Zhang, Y.; Fang, J.; Lu, K.; Wang, Z.; Ma, W.; Wei, Z. Conjugated Polymer-Small Molecule Alloy Leads to High Efficient Ternary Organic Solar Cells. *J. Am. Chem. Soc.* **2015**, *137* (25), 8176–8183.
(20) Huang, J.-H.; Velusamy, M.; Ho, K.-C.; Lin, J.-T.; Chu, C.-W. A ternary cascade structure enhances the efficiency of polymer solar cells. *J. Mater. Chem.* **2010**, *20*, 2820–2825.
(21) Savoie, B. M.; Dunaisky, S.; Marks, T. J.; Ratner, M. A. The Scope and Limitations of Ternary Blend Organic Photovoltaics. *Adv. Energy Mater.* **2015**, *5* (3), 1400891.
(22) Mai, J.; Lau, T. K.; Xiao, T.; Su, C. J.; Jeng, U.; Zhao, N.; Xiao, X.; Lu, X. Ternary morphology facilitated thick-film organic solar cell. *RSC Adv.* **2015**, *5* (107), 88500–88507.
(23) Liu, S.; You, P.; Li, J.; Li, J.; Lee, C.-s.; Ong, B. S.; Surya, C.; Yan, F. Enhanced Efficiency in Polymer Solar Cells by Adding a High-Mobility Conjugated Polymer. *Energy Environ. Sci.* **2015**, *8*, 1463–1470.
(24) Chen, M. C.; Liaw, D. J.; Huang, Y. C.; Wu, H. Y.; Tai, Y. Improving the efficiency of organic solar cell with a novel ambipolar polymer to form ternary cascade structure. *Sol. Energy Mater. Sol. Cells* **2011**, *95* (9), 2621–2627.
(25) Yang, L.; Zhou, H.; Price, S. C.; You, W. Parallel-like bulk heterojunction polymer solar cells. *J. Am. Chem. Soc.* **2012**, *134* (12), 5432–5435.
(26) Li, H.; Zhang, Z.-G.; Li, Y.; Wang, J. Tunable open-circuit voltage in ternary organic solar cells. *Appl. Phys. Lett.* **2012**, *101* (16), 163302.
(27) Khlyabich, P. P.; Rudenko, A. E.; Street, R. A.; Thompson, B. C. Influence of polymer compatibility on the open-circuit voltage in ternary blend bulk heterojunction solar cells. *ACS Appl. Mater. Interfaces* **2014**, *6* (13), 9913–9919.
(28) Yang, Y.; Chen, W.; Dou, L.; Chang, W.-H.; Duan, H.-S.; Bob, B.; Li, G.; Yang, Y. High-performance multiple-donor bulk heterojunction solar cells. *Nat. Photonics* **2015**, *9* (3), 190–198.
(29) Jeng, U. S.; Su, C. H.; Su, C.-J.; Liao, K.-F.; Chuang, W.-T.; Lai, Y.-H.; Chang, J.-W.; Chen, Y.-J.; Huang, Y.-S.; Lee, M.-T.; Yu, K.-L.; Lin, J.-M.; Liu, D.-G.; Chang, C.-F.; Liu, C.-Y.; Chang, C.-H.; Liang, K. S. A small/wide-angle X-ray scattering instrument for structural characterization of air–liquid interfaces, thin films and bulk specimens. *J. Appl. Crystallogr.* **2010**, *43* (1), 110–121.
(30) Dang, M.; Hirsch, L.; Wantz, G. P3HT:PCBM, Best Seller in Polymer Photovoltaic Research. *Adv. Mater.* **2011**, *23* (31), 3597–3602.
(31) Chao, Y. H.; Jheng, J. F.; Wu, J. S.; Wu, K. Y.; Peng, H. H.; Tsai, M. C.; Wang, C. L.; Hsiao, Y. N.; Wang, C. L.; Lin, C. Y.; Hsu, C. S. Porphyrin-incorporated 2D D-A polymers with over 8.5% polymer solar cell efficiency. *Adv. Mater.* **2014**, *26* (30), 5205–5210.
(32) Li, J.; Zhao, Y.; Tan, H.; Guo, Y.; Di, C.-A.; Yu, G.; Liu, Y.; Lin, M.; Lim, S.; Zhou, Y.; Su, H.; Ong, B. S. A stable solution-processed polymer semiconductor with record high-mobility for printed transistors. *Sci. Rep.* **2012**, *2*, 754.
(33) Xu, H.; Li, J.; Leung, B. H. K.; Poon, C. C. Y.; Ong, B. S.; Zhang, Y.; Zhao, N. A high-sensitivity near-infrared phototransistor based on an organic bulk heterojunction. *Nanoscale* **2013**, *5* (23), 11850–11855.
(34) Huang, Y.; Kramer, E. J.; Heeger, A. J.; Bazan, G. C. Bulk heterojunction solar cells: morphology and performance relationships. *Chem. Rev.* **2014**, *114* (14), 7006–7043.
(35) Chirvase, D.; Parisi, J.; Hummelen, J. C.; Dyakonov, V. Influence of nanomorphology on the photovoltaic action of polymer–fullerene composites. *Nanotechnology* **2004**, *15* (9), 1317–1323.
(36) Moon, J. S.; Jo, J.; Heeger, A. J. Nanomorphology of PCDTBT:PC70BM Bulk Heterojunction Solar Cells. *Adv. Energy Mater.* **2012**, *2* (3), 304–308.
(37) Liao, H.-C.; Ho, C.-C.; Chang, C.-Y.; Jao, M.-H.; Darling, S. B.; Su, W.-F. Additives for morphology control in high-efficiency organic solar cells. *Mater. Today* **2013**, *16* (9), 326–336.
(38) Liao, H.-C.; Chen, P.-H.; Chang, R.; Su, W.-F. Morphological Control Agent in Ternary Blend Bulk Heterojunction Solar Cells. *Polymers* **2014**, *6* (11), 2784–2802.
(39) Chang, S.-Y.; Liao, H.-C.; Shao, Y.-T.; Sung, Y.-M.; Hsu, S.-H.; Ho, C.-C.; Su, W.-F.; Chen, Y.-F. Enhancing the efficiency of low bandgap conducting polymer bulk heterojunction solar cells using P3HT as a morphology control agent. *J. Mater. Chem. A* **2013**, *1* (7), 2447–2452.
(40) Lu, X.; Hlaing, H.; Germack, D. S.; Peet, J.; Jo, W. H.; Andrienko, D.; Kremer, K.; Ocko, B. M. Bilayer order in a polycarbazole-conjugated polymer. *Nat. Commun.* **2012**, *3*, 795.
(41) Wu, W. R.; Jeng, U. S.; Su, C. J.; Wei, K. H.; Su, M. S.; Chiu, M. Y.; Chen, C. Y.; Su, W. B.; Su, C. H.; Su, A. C. Competition between fullerene aggregation and poly(3-hexylthiophene) crystallization upon annealing of bulk heterojunction solar cells. *ACS Nano* **2011**, *5* (8), 6233–6243.
(42) Chen, W.; Nikiforov, M. P.; Darling, S. B. Morphology characterization in organic and hybrid solar cells. *Energy Environ. Sci.* **2012**, *5* (8), 8045–8074.
(43) Patterson, A. L. The Scherrer Formula for X-Ray Particle Size Determination. *Phys. Rev.* **1939**, *56* (10), 978–982.
(44) Machui, F.; Rathgeber, S.; Li, N.; Ameri, T.; Brabec, C. J. Influence of a ternary donor material on the morphology of a P3HT: PCBM blend for organic photovoltaic devices. *J. Mater. Chem.* **2012**, *22* (31), 15570–15577.
(45) Street, R. A.; Davies, D.; Khlyabich, P. P.; Burkhart, B.; Thompson, B. C. Origin of the tunable open-circuit voltage in ternary blend bulk heterojunction organic solar cells. *J. Am. Chem. Soc.* **2013**, *135* (3), 986–989.
(46) Khlyabich, P. P.; Rudenko, A. E.; Thompson, B. C.; Loo, Y. L. Structural Origins for Tunable Open-Circuit Voltage in Ternary-Blend Organic Solar Cells. *Adv. Funct. Mater.* **2015**, *25* (34), 5557–5563.

DOI: 10.1021/acs.chemmater.6b02264
Chem. Mater. 2016, 28, 6186–6195

(47) Liu, F.; Zhao, W.; Tumbleston, J. R.; Wang, C.; Gu, Y.; Wang, D.; Briseno, A. L.; Ade, H.; Russell, T. P. Understanding the Morphology of PTB7:PCBM Blends in Organic Photovoltaics. *Adv. Energy Mater.* **2014**, *4* (5), 1301377.
(48) Sirringhaus, H.; Brown, P. J.; Friend, R. H.; Nielsen, M. M.; Bechgaard, K.; Langeveld-Voss, B. M. W.; Spiering, A. J. H.; Janssen, R. A. J.; Meijer, E. W.; Herwig, P.; de Leeuw, D. M. Two-dimensional charge transport in self-organized, high-mobility conjugated polymers. *Nature* **1999**, *401* (6754), 685−688.
(49) Tumbleston, J. R.; Collins, B. A.; Yang, L.; Stuart, A. C.; Gann, E.; Ma, W.; You, W.; Ade, H. The influence of molecular orientation on organic bulk heterojunction solar cells. *Nat. Photonics* **2014**, *8* (5), 385−391.
(50) Liao, H. C.; Tsao, C. S.; Lin, T. H.; Chuang, C. M.; Chen, C. Y.; Jeng, U. S.; Su, C. H.; Chen, Y. F.; Su, W. F. Quantitative nanoorganized structural evolution for a high efficiency bulk heterojunction polymer solar cell. *J. Am. Chem. Soc.* **2011**, *133* (33), 13064−13073.
(51) Liao, H.-C.; Tsao, C.-S.; Shao, Y.-T.; Chang, S.-Y.; Huang, Y.-C.; Chuang, C.-M.; Lin, T.-H.; Chen, C.-Y.; Su, C.-J.; Jeng, U. S.; Chen, Y.-F.; Su, W.-F. Bi-hierarchical nanostructures of donor−acceptor copolymer and fullerene for high efficient bulk heterojunction solar cells. *Energy Environ. Sci.* **2013**, *6* (6), 1938−1948.
(52) Liu, C.-M.; Su, Y.-W.; Jiang, J.-M.; Chen, H.-C.; Lin, S.-W.; Su, C.-J.; Jeng, U. S.; Wei, K.-H. Complementary solvent additives tune the orientation of polymer lamellae, reduce the sizes of aggregated fullerene domains, and enhance the performance of bulk heterojunction solar cells. *J. Mater. Chem. A* **2014**, *2* (48), 20760−20769.
(53) Pfeifer, P.; Ehrburger-Dolle, F.; Rieker, T. P.; González, M. T.; Hoffman, W. P.; Molina-Sabio, M.; Rodríguez-Reinoso, F.; Schmidt, P. W.; Voss, D. J. Nearly Space-Filling Fractal Networks of Carbon Nanopores. *Phys. Rev. Lett.* **2002**, *88* (11), 115502.
(54) Scherrenberg, R.; Coussens, B.; van Vliet, P.; Edouard, G.; Brackman, J.; de Brabander, E.; Mortensen, K. The molecular characteristics of poly(propyleneimine) dendrimers as studied with small-angle neutron scattering, viscosimetry, and molecular dynamics. *Macromolecules* **1998**, *31* (2), 456−461.
(55) Moon, J. S.; Takacs, C. J.; Sun, Y.; Heeger, A. J. Spontaneous formation of bulk heterojunction nanostructures: multiple routes to equivalent morphologies. *Nano Lett.* **2011**, *11* (3), 1036−1039.

DOI: 10.1021/acs.chemmater.6b02264
Chem. Mater. 2016, 28, 6186−6195